GAS RELATIVE PERMEABILITY REDUCTION DUE TO WATERBLOCKING – A LABORATORY BASED ANALYSIS

Catherine Laroche[1], Jairam Kamath, and Frank Nakagawa[2], Chevron Petroleum Technology Company, Ca, USA, and Yanis Yortsos, University of Southern California, USA

Abstract

We report results of a laboratory program to study the potential for waterblocking in a North Sea gas condensate reservoir. Waterblocking is caused by invasion of aqueous completion fluids and can reduce well deliverability. The laboratory data detailed in this paper was then used in a wellbore model to relate the reduced permeability of the near well-bore region to the gas saturation.[1]

The experiments consisted of humid methane injection into preserved core samples. We measured gas flow rate as a function of injected gas pore volume for several liquid systems and saturation states. The liquid systems comprised of brine, methanol, toluene, and brine-methanol mixtures. We injected over 10 000 PV of gas in each test to mimic near well bore conditions. The data showed that the liquid displacement regime was followed by a mass transfer regime, where evaporation causes the gas flow rate to slowly increase. It is in this regime that adding volatile fluids, such as methanol, to the completion brines has advantages.

The experimental data are analyzed to generate gas relative permeability curves using a model that accounted for both viscous displacement and evaporation effects. In the modeling of the evaporation process we clearly demonstrate that evaporation is driven by the pressure gradient across the sample. Even though the injected gas is humid, gas expansion causes water inside the core to be vaporized. This phenomena is very important in the near well bore environment where there are big pressure gradients and large volumes of gas flow.[1]

Introduction

Poor gas flow performance following well operations such as drilling, completions, and workovers was recently observed in some wells in a North Sea gas condensate field. Waterblocking from invasion of aqueous fluids was identified as a potential cause of low gas deliverability. The present work was conducted to evaluate the importance of waterblocking in this reservoir. We report on the laboratory data in this paper, and the results of mapping the laboratory data onto a well flow model to make gas deliverability predictions in SPE 63161.[1]

---

[1] Institut Français du Pétrole [2] Chevron Research Technology Company

Waterblocking has been suspected to reduce deliverability of gas reservoirs.[2-6] Bennion et.al.[2] and Cimolai et. al.[3] claim that water blocking is a problem where the in situ water saturation is significantly less than "irreducible" water saturation. They present two field case studies to advocate their claims. The first case study is on the Paddy formation in Central Alberta (k ~ 100 md; $f = 15\%$; $S_w(in\,situ) = 17\%$; $S_{wi}(lab) = 43\%$) The second is on the Cadomin formation in Alberta (k ~ 1md; $f = 5\%$; $S_w(in\,situ) = 20\%$; $S_{wi}(lab) = 52\%$). Metheven[4] discusses the performance of gas wells in the Frio and Wilcox formations in Texas. His data show that oil based drilling fluids lead to significant improvements in gas productivity compared to water based muds or invert emulsion. Laboratory tests indicate return permeabilities to gas after exposure to muds to be higher for oil-base mud compared to water-based mud. Metheven suggests water blocking and vaporization of oil base filtrate by gas production as reasons for these differences at the laboratory as well as field scale. Holditch [5] presents a numerical study of formation damage around a hydraulic fracture in a tight gas sand reservoir. He makes an interesting observation that formation damage can increase the capillary pressure of a rock and this synergetic effect could lead to waterblock problems. Abrams and Vinegar[6] use Computed Tomography to image the flow of nitrogen and brine in microdarcy gas sand cores. They claim that waterblock is unimportant if the drawdown pressure gradient in the region near a hydraulic fracture is of the order of several hundred psi/inch. Stimulation using alcohol or surfactants did not significantly improve gas flow in these cores.

Laboratory Experiments

We conducted laboratory experiments on a preserved, composite (3 plugs) sandstone sample with the following properties: $f = 16\%$, $k = 14$ md, $S_{wi} = 28\%$, $L = 16$ cm, $V_p = 30$ cc. The experiments consisted of a series of room condition, constant pressure drop humidified methane floods of the core sample containing various liquids (of brine, methanol, toluene, and brine-methanol mixtures) at two saturation states -- fully saturated with liquid, and containing liquid and trapped gas.

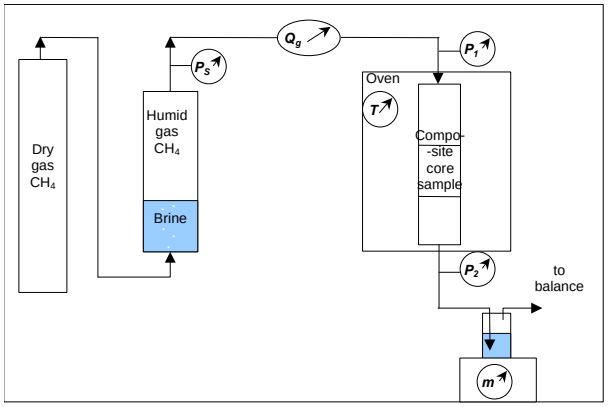

Figure 1: Schematic of experimental set-up

Experimental procedure Figure 1 presents a schematic of the experimental setup. The preserved core sample was flushed with toluene under backpressure, and the tests with toluene @Swi were conducted first. All the other sequence of tests using the different liquids (brine, methanol, iso-propanol, brine/methanol mixtures) began after flushing with cold methanol, flow through drying, and establishment of a 100% liquid state by flushing several pore volumes of the liquid under back pressure. Weight change of the core and absolute permeability are used to confirm the saturation state of the core.

The gas floods are all conducted by injecting humid methane from the top maintaining a constant pressure drop across the core sample of 10 psi. Dry methane out of the tank is humidified at ambient temperature in a humidification cell by flowing it through brine. The humidification cell allows adjustment of the upstream pressure required to deliver an increasing gas flow rate while keeping the pressure drop across the core constant. The outlet is open to the atmosphere, except for high-pressure experiments where a backpressure valve is used. Upstream, inlet and outlet pressures are constantly read with highly accurate piezoelectric transducers. A gas flow meter is placed between the reservoir cell and the inlet face of the core cell. The gas rate is re-calibrated to account for the deviation due to humid gas caused by higher resistance across a wet fritté. The liquid expelled at the outlet face is collected and its weight is monitored continuously. It is noted that liquid expulsion stops after a few pore volumes of gas injected, but the measured gas rate continues on increasing slowly. The flow test is stopped when the gas rate reached a maximum, and this is typically after about 1 to 3 weeks.

The core is then flooded with the same liquid at low rate so that significant trapped gas saturation remains. A new flow test is then conducted, by injecting humid methane into the core containing liquid at trapped gas saturation. Before saturating the core with a new liquid, it is cleaned by methanol flushes followed by flow through air drying.

Typical Measured data The measured data consists of gas flow rate, pore volumes gas injected, liquid expelled, and change in weight of the core at the end of each flood. Figure 2 presents a typical data set, where we have plotted the reduced gas flow rate (with respect to the maximum gas flow rate achieved in a dry core) and the liquid expelled as a function of PV_{gas}, the number of pore volumes of gas injected. The gas flow rate shows a rapid increase in the gas rate, corresponding to the liquid producing period, followed by a slow but continuous increase. The first period lasts at most 100-200 PV_{gas} and is referred to as the **displacement** regime. The second period, after liquid production has stopped but gas flow rate keeps increasing, corresponds to the **evaporation** regime, where non-displaced liquid is vaporized and carried out by the flowing gas.

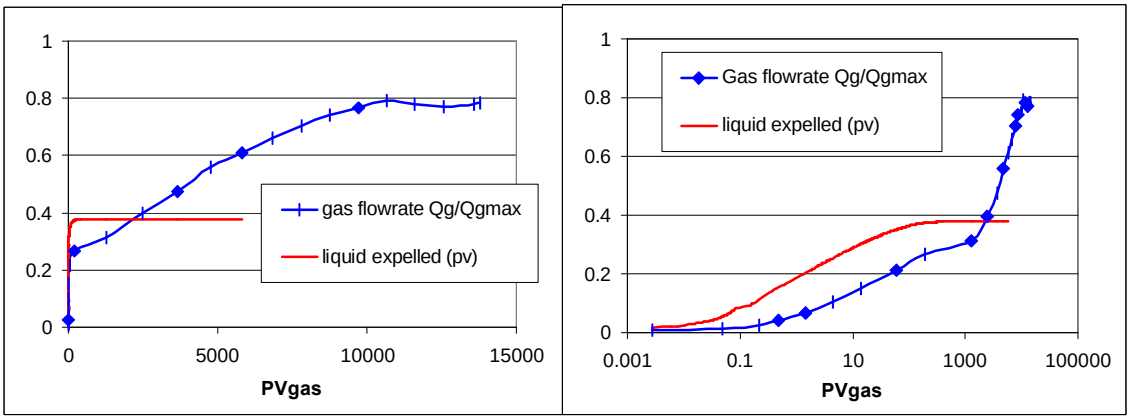

Figure 2: Gas flow rate and liquid expelled with pore volumes injected. KCl saturated core.

Only 30% of the dry core gas flow rate is recovered in the displacement regime. 10,000 PV_{gas} are needed in the evaporation regime to reach $Q_{g\max}$.

Model for calculating gas saturation

We require gas relative permeability data for modeling well performance.[1] The interpretation of the gas flow tests is based on successive displacement-evaporation regimes. For the displacement regime, the quantity of liquid displaced is measured, and the average gas saturation can be calculated. In contrast, the evaporation regime requires a model to predict the evolution of the gas saturation as function of number of pore volumes of gas injected.

In our experiments, the volatile liquid saturating the core contains one or two components (A and B). A non-condensable species C (gas) is injected at a pressure drop ΔP.

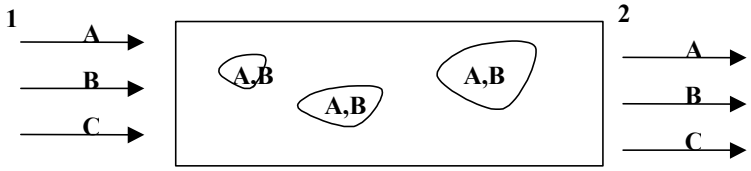

Figure 3: Schematic representation of the gas injection experiment: Non-condensable gas C injected in a core containing a volatile liquid (components A and/or B)

The evolution of saturation due to liquid displacement and evaporation is obtained by a combination of the mass balances over the condensable and the non-condensable components. For a binary system, where the liquid consists only of component A, the increment of gas saturation S_g as a function of time is given by

$$dS_g = \frac{dV_{l2}}{V_P} + \frac{M_A}{r_A}\frac{P_2}{z_2 RT}\frac{y_{A2} - y_{A1}}{1 - y_{A1}}dt_{PV} \qquad (1)$$

where dt_{PV} is the reduced time step, defined as,

$$dt_{PV} = \frac{Q_{g2}}{V_P} dt \tag{2}$$

Equation (1) requires molar fractions of component A to be known. The actual molar fraction can be related to the equilibrium molar fraction y_A^*, with the relative "humidity" ratio, defined as $H_A = \frac{y_A}{y_A^*}$. At ambient conditions, equilibrium molar fraction y_A^* can be determined from the saturation pressure p_A^* using Raoult's law with enough accuracy. For a binary system, Raoult's law yields $y_A^* = \frac{p_A^*}{P}$.

Equation (1) can then be expressed in terms of saturation pressure and relative "humidity" ratio of the volatile component as follow:

$$dS_g = \frac{dV_{l2}}{V_P} + \frac{M_A}{r_A} \frac{p_A^*}{z_2 RT} \frac{(H_{A2} - H_{A1})P_2 + H_{A2}\Delta P}{P_1 - H_{A1} p_A^*} dt_{PV} \tag{3}$$

Equation (3) clearly demonstrates that evaporation is driven by the pressure gradient ΔP across the sample. Even though the injected gas is 100% saturated $(H_{A1} = H_{A2} = 1)$, water inside the core will be vaporized, because of the gas compressibility. From equation (3) we can see that vaporization also depends on the absolute pressure, and would therefore not be really favored at reservoir conditions, even though the saturation pressure p_A^* increases with temperature.

The model for a ternary system is in the appendix.

Determination of gas relative permeability curves

We applied our model to the different gas/liquid data sets. Injected gas in all cases is humid methane, whereas liquid initially in place in the sample is one of the following:

- *aqueous liquids*: brine (3% KCl), mixtures of brine and methanol (30% and 50% volume of methanol, referred to as KCl-MeOH 3:1 and KCl-MeOH 1:1 respectively).
- *other liquids*: toluene (in presence / absence of Swi), methanol, isopropanol.

Table 1 gives an overview of the saturation pressures and humidity ratios for the different systems.

		Binary systems			
Liquid component		**KCl** (Brine)	**MeOH** (Methanol)	**IPA** (Isopropanol)	**Toluene**
Saturation pressure at 70ºF: p_A^*, psia		0.46	2.44	0.83	0.55
Humidity ratio at inlet H_{A1}		0.4-1	0	0	0
		Ternary systems			
Liquid mixture		**KCl-MeOH 3:1** (mixture at 30% vol. of MeOH)		**KCl-MeOH 1:1** (mixture at 50% vol. of MeOH)	
Equilibrium partial pressure at 70ºF, psia	p_{KCl}^*	0.27-0.46 (depends on the fraction of methanol in		0.27-0.46 the liquid which varies from 30% to 0%)	
	p_{MeOH}^*	0-0.63 (depends on the fraction of methanol in		0-0.96 the liquid which varies from 30% to 0%)	
Humidity ratio at inlet	H_{KCL1}	0.4-1		0.4-1	
	H_{MeOH1}	0		0	

Table 1: Values of partial pressure and humidity ratio for the different liquids considered

The humidity ratio relative to non-aqueous component is always zero since the injected gas is only saturated with water. The humidity ratio relative to the water component departs from unity as experiment progresses. This is because the gas flow rate increases and the pressure of the humidification cell becomes increasingly higher than the core inlet pressure.

Sample fully saturated with liquid Figure 4 plots the relative permeability curves $Kr_g = f(S_g)$ obtained for the different liquid systems. The gas relative permeability is an average, $\overline{Kr}_g = \dfrac{U_g m_g}{k \cdot \Delta P / L}$. The gas saturation is an average S_g, and is calculated from the produced liquid data in Figure 4a (pure displacement), and from equation 3 for Figure 4b (displacement + vaporization). Two important features of the data are that the Kr_g curves do not collapse and there is significant residual liquid saturation at the end of the displacement regime. We show below that viscosity ratio, local versus average curves, capillary end effects or core level viscous fingering do not explain these features. This leaves us with the hypothesis that this may be due to pore-level bypassing of liquid during gas-liquid displacements, or gas wetting features present in the reservoir rock. This hypothesis is supported by the heterogeneous nature of the rock facies and the presence of bitumen in some of the pores of this rock type.

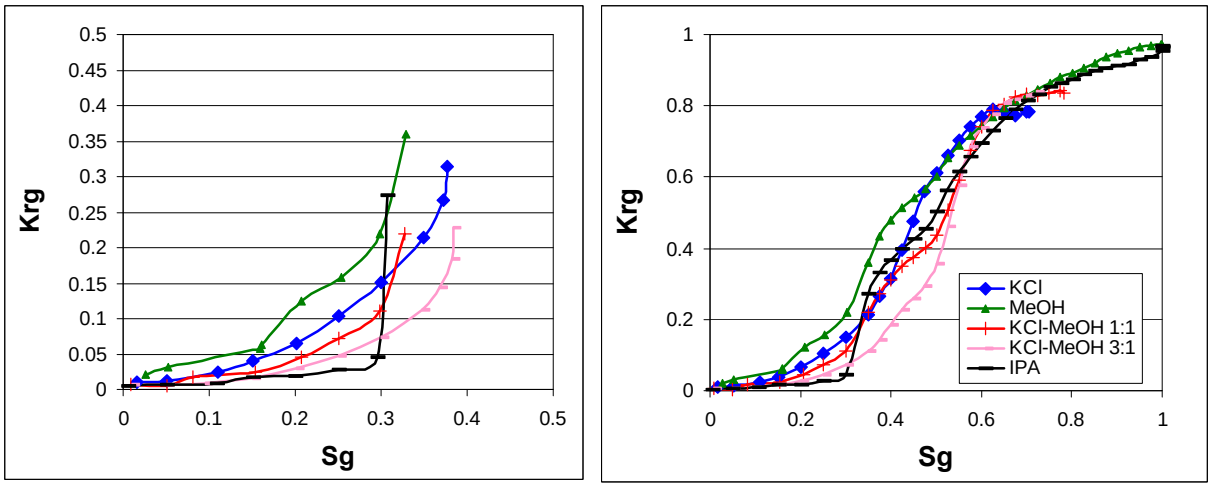

Figure 4: Average relative permeability $\overline{Kr}_g = \dfrac{U_g m_g}{k \cdot \Delta P / L}$ *as a function of gas saturation* S_g

(a) S_g *: displaced liquid only* **(b)** S_g *: displaced + vaporized liquid*

Viscosity ratio effects The curves in figure 4a do not collapse, although the gas permeability curve $Kr_g = f(S_g)$ is typically expected to be independent of the fluid system. We conducted two experiments with methanol, one with toluene @ S_{wi}, and one with toluene, and these curves overlay each other. This observation could suggest a dependence of the Kr_g curves with the viscosities of the liquid, since toluene and methanol have the same viscosity. The other liquids have higher viscosity and shows lower values of Kr_g for a given gas saturation S_g. However, if we consider the same set of relative permeabilities for each fluid systems, an analysis based on Buckley-Leverett displacement does not show any effect of the viscosity ratio M (where M ranges between 50 and 230) on the average gas flow rate vs. $\overline{S}_g$ curve. The reported data is an average curve, but the average curve is the same as the local Kr_g-S_g curve, if we assume a Buckley-Leverett displacement. This assumption is correct provided that capillary end effects are negligible.[8]

Large Residual Saturation There is a large residual liquid saturation ~ 65% PV at the end of the displacement regime. The main issue is whether capillary end effects are not the cause of these high residual values – (i) the dimensionless ratio of viscous to capillary forces at the core level[7] $N_{RL} = \dfrac{\Delta P}{P_C} \approx \dfrac{\Delta P}{g}\sqrt{\dfrac{k}{f}}$ equals 0.6, and this is below the value that should effect end point saturation values; [7] (ii) indicating no strong predominance of the capillary forces at the core scale. This is corroborated by the results of floods conducted

at 10 psi and 20 psi pressure drops which demonstrates the same $Kr_g - PV_{gas}$ behavior during the displacement period; and (iii) fractional liquid flow rates at the outlet demonstrate a power-law behavior $f_l \propto t^{-a}$ consistent with predominance of viscous forces.[8]

We also used NMR imaging to confirm that capillary end effects or core scale viscous fingers were not the cause of the high residual liquid saturation. Figure 5 shows that there in no gradient in the saturation profiles in either direction (axial or radial). This shows that there are no capillary end effects or viscous fingers.

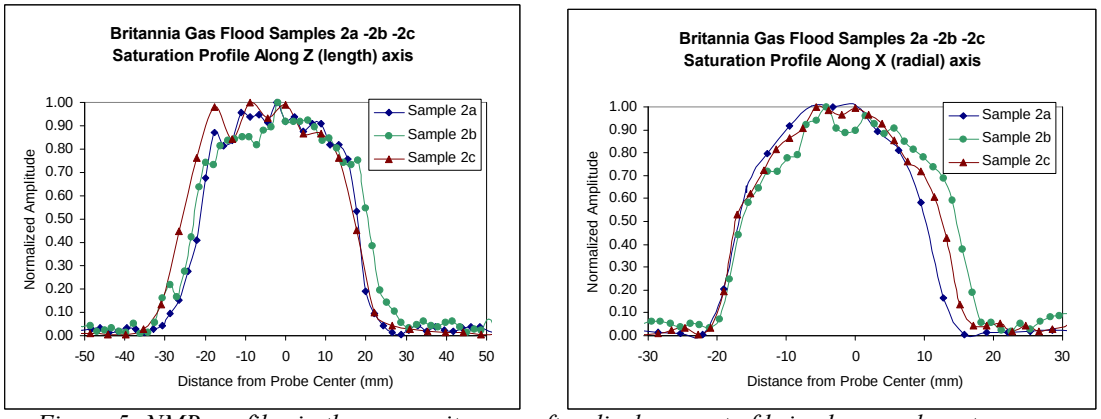

Figure 5: NMR profiles in the composite core after displacement of brine by gas along two axes
(a) *Z axis - length* **(b)** *X axis - radial*

High S_g data At higher saturation, during the evaporation regime, figure 4b shows that the curves follow the same trend. The predicted final gas saturation is checked at the end of flow test experimentally evaluated by weighing the sample.

Sample with trapped gas Figure 6 presents the gas relative permeability as a function of the gas saturation predicted according to the displacement-evaporation model (equation 3).

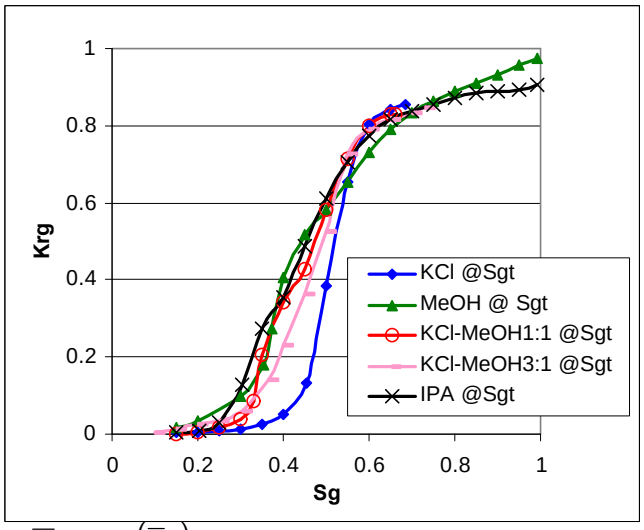

Figure 6: $\overline{Kr}_g = f\left(\overline{S}_g\right)$ *for different fluid systems with initial trapped gas*

There are two important differences in the shape of the Kr_g curves for the trapped gas case compared to the saturated liquid case. The experiments in the trapped gas case are conducted with varying initial trapped gas saturation. This creates a much more important divergence in the Kr_g vs. S_g curves in the displacement regime. Also, volatilities of the liquids is more important in the trapped gas case. The small amount of evaporation during the displacement phase can be sufficient to vaporize rings of liquid separating the trapped gas from the displacing gas. Although these rings may not be important in term of volume of liquid vaporized, their disappearance allows the trapped gas to progressively reconnect to the flowing gas phase. This mechanism leads to an increase of the flowing gas saturation and as a result to an increase of the gas permeability.

Comparison between saturated / trapped gas data Figure 7 compares results for the KCl-Methanol 1:1 liquid system with and without initial trapped gas. It is shown on figure 6a that curves diverge at lower saturation (displacement regime) and then more or less converge at higher gas saturation. The divergence during the displacement regime corresponds to the initial trapped gas quantity S_{gt}^i. By plotting $\overline{Kr}_g$ as a function of $\left(\overline{S}_g - S_{gt}^i\right)$, the curves from experiments at S_{gt}^i and at $S_{gt}^i = 0$ collapse at low S_g. This implies that the injected gas first invades the core as if it were completely saturated with liquid and there were no trapped gas. At bigger values of $\left(\overline{S}_g - S_{gt}^i\right)$, the Kr_g curves are higher in the trapped gas system because volatilization of the rings separating the flowing and initial trapped phases causes rapid increases in the flowing gas phase saturation.

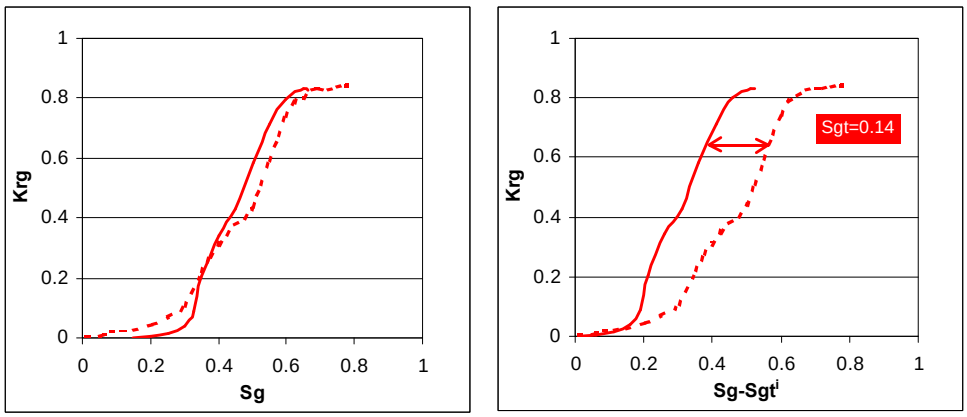

Figure 7: Comparison of $\overline{K}_{rg}$ *vs.* **(a)** *total gas saturation* $\overline{S}_g$ *;* **(b)** *vs. flowing gas saturation* $\left(\overline{S}_g - S_{gt}^i\right)$ *for KCl-MeOH 1:1 systems with (bold solid line) and without (dashed solid line) initial trapped gas*

Conclusions

1. The gas flow rate exhibits a two region behavior -- rapid increase during the liquid producing period (displacement regime) and then a slow but continuous increase (evaporation regime).
2. The displacement regime is completed after 10 to 50 PV of gas are injected. Here the flow rate increases to about 20-30% of the gas rate in clean, dry samples.
3. The residual liquid saturation at the end of the displacement regime is high (65-70%). Uniform liquid saturation profile observed by NMR together with a theoretical analysis prove that this is not due to capillary end effects or viscous fingering.
4. The gas relative permeability curves in the displacement regime are identical for saturated methanol, toluene, and toluene @ S_{wi} systems. These data are different from the gas relative permeability curves for the aqueous systems.
5. The evaporation regime is long and can require more than 10 000 PV of injected gas. Our model of the evaporation process clearly demonstrates that evaporation is driven by the pressure gradient across the sample.
6. The data suggest a conceptual model where gas floods into saturated liquid cores bypasses liquid blobs, leading to high residual liquid saturation that are then slowly volatilized in the evaporation regime. In the trapped gas case, evaporation of the thin liquid rings separate the flowing and trapped gas phases lead to sharp increase in flowing gas saturation.

Nomenclature

Ca : capillary number
CA : macroscopic capillary number
Kr_g : gas relative permeability
L : length of the core
M_A : molecular weight of component A,
P : outlet pressure,
Q_g : gas flow rate
R : universal gas constant,
S_g : gas saturation
S_{gt}^i : initial trapped gas saturation
S_{wi} : irreducible water saturation
T : temperature,
V_P : total pore volume,
dt_{PV} : reduced time step,
dV_{l2} : volume of liquid expelled at each time step,
f_l : liquid fractional flow rate
U_g : gas velocity
r : typical size of a pore radius
y_A : molar fraction in the gas of component A,
y_A^* : equilibrium molar fraction in the gas of component A,
z : gas deviation factor at outlet conditions,
μ_g : gas viscosity,
ρ_A : mass density of component A,

Subscript: 1: inlet - 2: outlet

References

1. Kamath J., Laroche C., and Nakagawa F., " Laboratory Based Evaluation of Gas Well Deliverability Loss Due to Waterblocking," paper SPE 63161 to be presented at the 2000 SPE Annual Technical Conference, Dallas, TX, October
2. Bennion, D. B. et. al., "Reductions in the Productivity of Oil and Gas Reservoirs due to Aqueous Phase Trapping, " paper CIM93-24 presented at the CIM 1993 Annual Technical Conference, Calgary, May 9-12
3. Cimolai, M. P. et. al., " Mitigating Horizontal Well Formation Damage in a Low-Permeability Conglomerate Gas Reservoir," paper SPE 26166 presented at the 1993 SPE Gas Technology Symposium, Calgary, June 28-30
4. Methven, N. B. "Effects of Drilling Fluids on Gas Well Productivity," paper SPE 3504 presented at the 1971 SPE Annual Fall Meeting, New Orleans, Oct. 3-6
5. Abrams, A. and Vinegar, H. J. "Impairment Mechanisms in Vicksburg Tight Gas Sands," paper SPE/DOE 13883 presented at the 1985 SPE/DOE Joint Low Permeability Symposium, Denver
6. Holditch, S. A., " Factors Affecting Water Blocking and Gas Flow From Hydraulically Fractured Gas Wells," Journal of Petroleum Technology, Dec 1979, pp 1515-1524
7. Kamath, J., deZabala, E.F. and Boyer, R.E." Water/Oil Relative Permeability Endpoints of Intermediate-Wet, Low Permeability Rocks," SPEFE, March 1995
8. Laroche C., Yortsos Y.C. and Kamath J., " Time Scaling of Produced Fluid Rates in Laboratory Displacements," to be presented at the 2000 European Conference on Mathematics for Oil Recovery, Italy, October

Appendix

Model for ternary system - When two volatile components A and B are present in the liquid, the system is ternary. Similarly to binary systems, the increment of gas saturation dS_g at each time step can be split into three different contributions:

- amount of liquid expelled by displacement:

$$-dS_{l-displaced} = \frac{dV_{l2}}{V_P} \tag{4}$$

- amount of component A vaporized from the liquid to the gas phase:

$$-dS_A = \frac{M_A}{r_A}\frac{P_2}{z_2 RT}\frac{\left[y_{A2} - y_{A1} + y_{A1}y_{B2} - y_{B1}y_{A2}\right]}{1 - y_{A1} - y_{B1}}dt_{PV} \tag{5}$$

- amount of component B vaporized from the liquid to the gas phase:

$$-dS_B = \frac{M_B}{r_B}\frac{P_2}{z_2 RT}\frac{\left[y_{B2} - y_{B1} + y_{B1}y_{A2} - y_{A1}y_{B2}\right]}{1 - y_{A2} - y_{B2}}dt_{PV} \tag{6}$$

The total increment of gas saturation during each reduced time step dt_{PV} is the sum of the three contributions:

$$dS_g = -dS_{l-displaced} - dS_{lA} - dS_{lB} \tag{7}$$